GI_Forum 2023, Issue 1
Page: 45 - 68
Full Paper
Corresponding Author:
jarrettinho@yahoo.co.uk
DOI: 10.1553/giscience2023_01_s45

SAR Change Detection to Evaluate Flood Event Characteristics, Pre- and Post-Restoration of a Floodplain

Sean Jarrett[1], Daniel Hölbling[1]
[1]University of Salzburg, Austria

Abstract

A method using Sentinel-1 synthetic aperture radar (SAR) data to evidence flood changes after floodplain restoration is proposed. A Natural Flood Management (NFM) project on the Ouse river in southern England, undertaken by the Sussex Flow Initiative, was analysed to ascertain any reduction of previous flood risk. GIS operations were conducted on the results of the change detection analysis to identify how flood area, form and compactness were affected after the NFM installation, and how these changes relate to the project aims. Flood records based on internet-published drone footage verified the change detection methodology. A scorecard was developed to evaluate the benefits and disadvantages of spatial changes seen in post-restoration floods in comparison to inundation before the measures were installed. Evaluation results were used in the annual report of the SFI project to demonstrate the attenuation of floodwaters in accordance with the aims of the project.

Keywords:

natural flood management, Sentinel-1, change detection, synthetic aperture radar (SAR)

1 Introduction

Natural Flood Management (NFM) slows river flow and stores floodwaters. It is a flood defence technique that is gaining consideration in flood risk planning and environmental policy (Environment Agency, 2020; HM Government, 2018). However, a lack of reliable evidence as to the performance of NFM installations hinders advocating its more widespread use in flood defence (Bernhardt et al., 2005; Environment Agency, 2018; van Rees et al., 2022).

Remote sensing has been extensively used to detect flooding (Klemas, 2015). Synthetic aperture radar (SAR) technology penetrates cloud cover that is prevalent during flood events (Huang, Chen, Zhang, & Wu, 2018; Zhou et al., 2017) and detects inundated vegetation (Kasischke, Melack, & Craig Dobson, 1997). SAR flood detection, however, can be affected by surface roughness caused by wind (Carreño Conde & De Mata Muñoz, 2019; Manjusree, Prasanna Kumar, Bhatt, Rao, & Bhanumurthy, 2012), and radar shadow and foreshortening (Cian, Marconcini, & Ceccato, 2018).

Empirically defined thresholds cannot be used to detect floodwaters due to the changing characteristics of surface features (Martinis & Rieke, 2015). Using temporal comparison to detect flooded areas has demonstrated consistently good results (Brivio, Colombo, Maggi, & Tomasoni, 2002). Change detection requires that all variables other than the variable of interest are constrained as far as possible (Green, Kempka, & Lackey, 1994; Lu, Mausel, Brondízio, & Moran, 2004; Singh, 1989). Various change detection techniques have been applied in monitoring natural processes such as flooding (Macleod & Congalton, 1998; Matgen et al., 2011). The specificities of NFM installations render them particularly suitable for the use of change detection and thresholding (CDAT), which has been successfully used in flood mapping research (Clement, Kilsby, & Moore, 2018; Long, Fatoyinbo, & Policelli, 2014).

This study proposes the use of remotely sensed SAR imagery to enhance the evaluation of NFM schemes through CDAT inundation delineation and the assessment of changes in spatial characteristics of flooding. Taking into account the aims of the NFM project, spatial analysis focuses on changes in the overall inundation area, the form of floodwaters in relation to the design intent of the management measures, and containment of flooding in terms of compactness. The methodology is relevant to NFM projects in being portable, scalable and replicable.

The study aim is to apply SAR change detection to evaluate the effects of floodplain restoration on the characteristics of flood events before and after implementation. Key objectives are:

1. To select a suitable project that has used NFM measures on a floodplain to attenuate floodwater and thereby create beneficial changes to flood characteristics.
2. To select SAR imagery for pre- and post-restoration flood events that are comparable in terms of seasonality, flood peak and weather conditions which may affect SAR sensitivity.
3. To undertake an accuracy assessment in order to verify the performance of the thresholding technique in detecting floodwater extent.

2 Methodology

Most NFM projects have been developed by third-sector environmental organizations with limited budgets, where evaluation resources have historically been limited. Use of open data sources and software has therefore been embedded into the methodology to develop an evaluation process for application on similar future projects. CDAT analysis of SAR satellite imagery was employed, using the image difference technique to detect floodwaters and inundated vegetation.

Sets of temporal data were compiled to represent pre- and post-NFM installation floods, allied with a baseline reference image for each event when the river was at a seasonally-similar average level. River level and flow records from the nearest official gauging stations to Cockhaise Brook were consulted in order to identify comparable significant peaks. These data

allowed the evaluation of how flood events may have changed locally due to the introduction of NFM measures.

Research objectives followed defined change detection principles (Lu et al., 2004), focusing on:

- Change in the total area of floodwater.
- Spatial distribution of changes in flooding, focusing on any relationship between the post-NFM flood form and the location of measures implemented, plus the compactness of the overall extent of the flood.
- Accuracy assessment, verified by applying the detection methodology locally in Sussex (where known flooding occurred on specific dates) for use as a ground truth reference.

2.1 The Study Area

The Sussex Ouse is a river system in southern England running from the sandstone High Weald, through chalk downland, and into the English Channel at Newhaven. Cockhaise Brook is approximately 8 km long and joins the Ouse in relatively hilly terrain, through a more varied geological landscape of Wadhurst clay and the start of the High Weald sandstone.

The Sussex Flow Initiative (SFI) is a multi-agency project that has installed NFM measures in the Ouse catchment to reduce flood risk by re-engaging the floodplain. The area of interest (AOI; Figure 1) is a series of features situated on Cockhaise Brook at Woodsland Farm, near the town of Haywards Heath in West Sussex. The principal project aim is to reduce local flood risk around the now-residential Cockhaise Mill area.

Figure 1: The Cockhaise Brook AOI including NFM

The main measures installed were two 'Run-off Attenuation Features', more commonly referred to as scrapes, both approximately 500m² in area. Figure 2 shows the primary scrape, partially flooded, in early spring 2022.

Figure 2: The primary scrape installed on reconnected floodplain adjacent to Cockhaise Brook in order to attenuate floodwaters.

2.2 Data Acquisition

The pre-NFM data extended from when Sentinel-1 imagery first became available in April 2014 until December 2018, when the first NFM features were installed. The temporal window for post-restoration data was from October 2019, when the final NFM feature was installed, onwards. In accordance with change detection principles to control as many input variables as possible, comparable datasets were selected based on the same satellite pass time (ascending or descending) and similar wind conditions/direction.

At the nearest gauging station to Cockhaise Brook, 6 km downstream at Freshfield Bridge on the Ouse, river level records for the pre-NFM period show the highest average recorded was 1.75m on 11 January 2016. The blue zone in Figure 3 illustrates the short peak window in which SAR imagery could be used (10–13 January 2016). A baseline date was selected from the period shown in green, when the river was at a consistently low level.

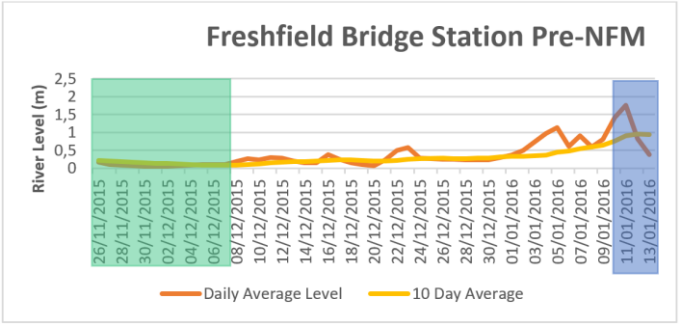

Figure 3:
Daily average levels recorded at Freshfield Bridge gauging station around the highest pre-NFM period flood peak.

Sentinel-1 imagery was available for 10 January (recorded level 1.41m compared with the 1.75m peak on 11 January) in a descending pass, and for 13 January in an ascending pass (recorded level 0.39m). Both dates had the potential to reveal different insights into the flood: 10 January provided the fourth highest recorded level in the pre-NFM period; 13 January gave a snapshot of the flood dissipation. Local weather records show relatively strong south-easterly winds on both dates.

Table 1 shows the compatibility of the satellite specification and wind conditions images representing baseline state and flood event scenarios.

Table 1: Summary of key data for the selected flood and dry dates for the pre-NFM period.

Satellite Specification	Flood Date	Conditions	Wind Speed/Direction
Sentinel-1 6am descending pass	10 January 2016	Flood	35 km/h SE
	5 December 2015	Dry	41 km/h SE
Sentinel-1 6pm ascending pass	13 January 2016	Flood	22 km/h S
	26 November 2015	Dry	15 km/h SW

The highest post-NFM flood peak recorded at Freshfield Bridge was on 20 December 2019 (daily average 2.31m). This was a substantial event, as the highest ever daily average recorded at the station was 2.63m, in January 2008. As no comparable data for pre-NFM floods exist, the data for around 20 December 2019 (shown in purple in Figure 4) could be used only to assess detection accuracy at local ground truth sites.

The next largest post-NFM flood occurred on 27 November 2019, with a daily average of 1.77m, comparable to the January 2016 event. Suitable dates around this peak are shown in blue. Potential baseline data periods are shown in green.

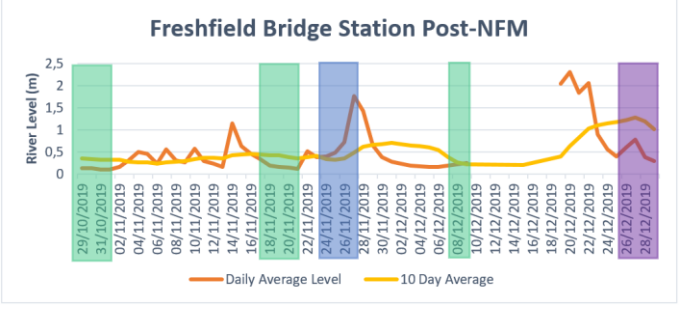

Figure 4:
Daily average levels recorded at Freshfield Bridge around the highest post-NFM period flood peak.

Sentinel-1 imagery in a descending pass was available for 27 November 2019, at the flood's peak. Local weather records show very strong easterly wind speeds of 64 km/h on this date.

Table 2 shows the compatibility of the selected post-NFM datasets in terms of satellite specification and wind conditions.

Table 2: Summary of key data for the selected flood and dry dates for the post-NFM period.

Satellite Specification	Date	Conditions	Wind Speed/Direction
Sentinel-1B 6am descending pass	27 November 2019	Flood	64 km/h E
	9 December 2019	Dry	57 km/h S

2.3 Pre-Processing Procedures

Sentinel-1 satellites operate in C-band wavelength radar waves in Interferometric Wide (IW) mode, with dual polarization. Signals are therefore emitted in vertical polarization; backscatter responses are recorded in vertical or co-polarization (VV), and horizontal or cross polarization (VH). Level 1 Ground Range Detected (GRD) data products with a high-resolution were acquired. Prior to release, these datasets had been multi-looked and projected based on an ellipsoid model of the Earth.

Pre-processing was carried out using European Space Agency SNAP software, based on the following specification:

- Orbit State Vectors (OSV)
    - Recommended SNAP parameters of Sentinel Precise OSVs and 3rd polynomial degree were used to improve geographic accuracy (Bioresita, Puissant, Stumpf & Malet, 2018).
- Removal of thermal noise
- Calibration
    - GRD pixel digital numbers were calibrated to Sigmaθ values, which provide the best separation between water and land (Bioresita et al., 2018).
- Terrain Correction
    - The SRTM DEM (30m) was used to geocode the images using bi-linear interpolation and nearest-neighbour resampling.
    - Pixel resolution was 10m azimuth x 10m range.
    - A WGS 84 geographic projection was used for the terrain correction.
- Speckle Filter
    - A Gamma MAP filter was applied to replicate the Long et al. (2014) methodology.
    - The Lee filter, which has been proved to reduce false positive rates (Carreño Conde & De Mata Muñoz, 2019), was tested against Gamma MAP.
    - As the AOI is very small, a 3x3 filter size was used.

2.4 Change Detection GIS Workflow

After pre-processing, the raster Sigmaθ datasets of dry and flood images were manipulated and analysed in QGIS, as shown in Figure 5.

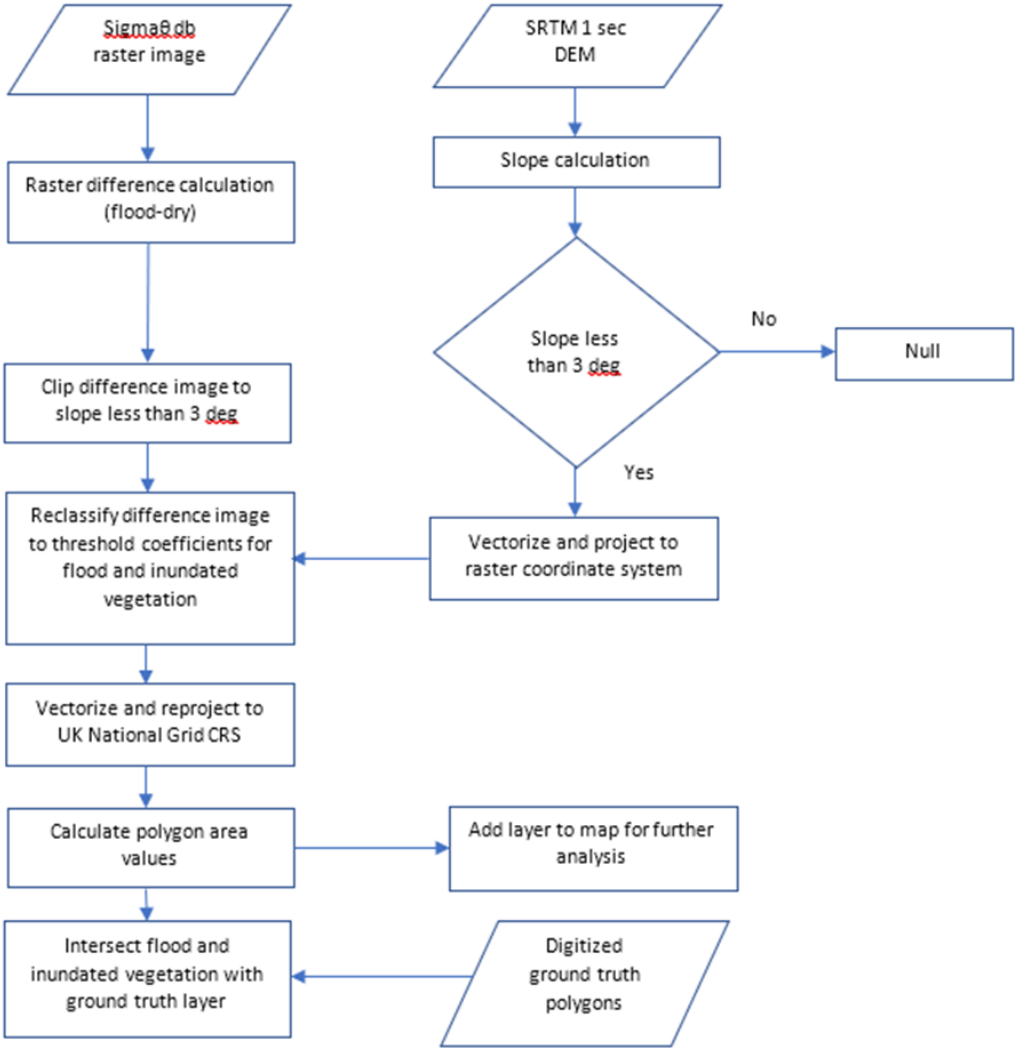

Figure 5: GIS workflow for detection of flood inundation change.

The QGIS raster calculator tool created a new raster layer of the difference between the flood and dry values, which was then clipped by a mask layer of all slopes of less than 3 degrees. The mask layer removes the possible effects of shadow in hilly terrain producing false positives (Clement et al., 2018). Replicating the parameters used by Long et al. (2014), pixel values with

a slope of more than 3 degrees were removed from the difference image using the SRTM DEM.

The mean and standard deviation values from the resultant masked image difference layer were then used to formulate histogram thresholds to define open floodwater and inundated vegetation pixels.

2.5 Histogram Thresholding

Long et al.'s (2014) formula (formula 1 below) was applied to the Sigmaθ dB of flood minus reference values, where slope is less than 3 degrees, to classify open floodwater pixels:

$$P_{DF} < (\{lmean[D] - k_f * [D]\}) \quad (1)$$

where P_D is the floodwater pixels, *lmean* the mean of the difference image, *lσ* the standard deviation of the difference image, and k_f the coefficient value. All pixel values below the P_{DF} value are classified as flooded.

The threshold formula to identify inundated vegetation is as per Long et al. (2014):

$$P_{DI} > (\{lmean[D] + k_f * [D]\}) \quad (2)$$

Here, all pixel values above the P_{DI} value are classified as inundated vegetation.

The threshold values slice the tails of the Sigmaθ dB difference image histogram into detected floodwaters and inundated vegetation, as shown by the orange lines in Figure 6 for the 21 December 2019 flood and reference date of 20 November 2019. Using the image difference mean (shown by the red line) and standard deviation (shown by the green lines) ensures that these thresholds are 'sensitive' to the land cover depicted, making the method applicable to most landscapes (Long et al., 2014).

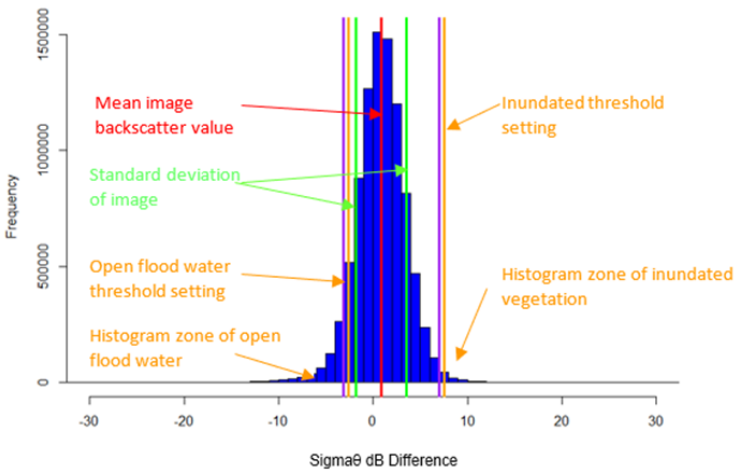

Figure 6: Histogram of Sigmaθ dB values for the difference image of the 21 December 2019 flood and 20 November reference.

The thresholds identify changes in radar backscatter between the baseline and flood images. For open floodwaters, the baseline image depicts surface roughness, such as vegetation. In the flood image, inundated areas have very low backscatter values, due to the submerged land acting as a specular reflector. The resultant large negative differences in Sigmaθ dB values therefore indicate a change in state from vegetation to flood conditions. Conversely, inundated vegetation, for example where grass, crops etc. protrude above the floodline, is identified by large differences in Sigmaθ dB values because the reflecting effect of water below the herbaceous cover increases the scattering of radar waves. Below a minimum depth of cover between the top of the protruding vegetation and the floodwater level, Sigmaθ dB values can start to decrease as the vegetation becomes less disruptive in scattering reflected radar waves (Zhang, Wdowinski & Gann, 2022).

2.6 Ground Truth Sampling

The accuracy assessment used ground truth sample sites with the following characteristics:

- predominantly natural surfaces to replicate the landscape around the SFI project;
- in terrain with a slope of less than 3 degrees;
- flood reference sites that may be susceptible to fluvial inundation but that are not permanently flooded in wet periods. The CDAT method is reliant on seasonally similar dry and flood datasets to limit the effect of change due to the agricultural cycle;
- dry reference sites that even in high magnitude events do not flood.

The most reliable records that could be used as ground truth data was drone footage, published on YouTube, of the substantial December 2019 floods in Sussex. Drone film material for various sites on the Ouse and other Sussex rivers around this period was used to digitize flood extent in QGIS from a Google Map base layer. Samples of dry areas where it could reasonably be assumed that no breach occurred were also digitized. There is, however, an accepted possibility that these areas were inundated after the footage was taken.

An array of 22 suitable ground truth samples were used from 6 different sites across Sussex. Table 3 sets out the temporal and locational issues in using these samples. Euclidean distances from the NFM features provide context as to the variance in distance of each sample from the AOI.

CDAT analysis was conducted on the ground truth sites on the consecutive days of 20 and 21 December 2019 to capture the backscatter effects of different wind conditions for these dates.

To ensure that the optimum threshold parameters were applied, a range of threshold values were classified in the flood/dry difference image for the ground truth samples. Based on the CDAT criterion (Long et al., 2014), coefficients ranging from 1 to 1.5 for floodwaters and 2 to 2.5 for inundated vegetation were used to identify optimum histogram threshold values.

Table 3: Temporal and locational variances for the selected ground truth sample sites.

Ground Truth Sample Location	Euclidean Distance from SFI Site (km)	River/stream	Area (ha)	River Gauging Station	Flood Record Sample Date	Variance to Flood Peak on 20/12/19 (Days)
Anchor Inn, Barcombe	13	Ouse	1.2	Anchor Gates	20/12/19	0
Great Walstead	2	Scrase (stream), Ouse	9.7	Freshfield Bridge	22/12/19	2
Alfriston	28	Cuckmere	33.3	Sherman Bridge	22/12/19	2
Hellingly	26	Bull	18.4	Leabridge	27/12/19	7
Mock Bridge, Henfield	19	Adur	79.8	Sakeham Weir	22/12/19	2
Wineham	15	Adur	80.7	Sakeham Weir	20/12/19	0

2.7 Evaluation of Flood Characteristic Changes Post-NFM Installation

An evaluation of the NFM features on Cockhaise Brook was undertaken to assess how comparable flood events before and after installation of flood management measures differed in terms of spatial characteristics. To aid evaluation, the catchment was broken down into identified functional zones, as shown in Figure 7, based on the following:

- Zone 1 – the furthest upstream zone, including a road that can be breached by flooding and the confluence of a stream with Cockhaise Brook, which may be affected by the NFM measures during high flows.
- Zone 2 – the area immediately upstream of the main NFM scrapes, comprising smaller-scale floodplain reconnections and Black Poplar trees planted to improve soil drainage.
- Zone 3 – the main NFM scrapes and their immediate vicinity, designed to attenuate large volumes of floodwater.
- Zone 4 – this was divided into two to take account of the effect of Holywell weir.
    - Zone 4a – immediately downstream of the main scrapes to the confluence with Danehill Brook, below which is the weir. Flood extent and spatial form could be affected by upstream attenuation in the main scrapes. There are also areas of planted Black Poplar.
    - Zone 4b – immediately downstream of Holywell weir. A smaller scrape has been formed here, along with more planting of Black Poplar trees.
- Zone 5 - the main aim of the SFI project is to mitigate flooding around the Cockhaise Mill site. Changes in flood area and form in this location will indicate how successful the upstream NFM features have been in mitigating and diverting floodwaters away from the mill.

- Zone 6 – the stretch of Cockhaise Brook immediately to the north of the confluence with the Ouse.

Zones were delineated to the east of the brook by a railway embankment, and to the west by hilly terrain. Only flooding located between the brook and these features was considered as having a possible causal relationship with the NFM features. A greater zonal area was also included to focus on the vicinity of the NFM features.

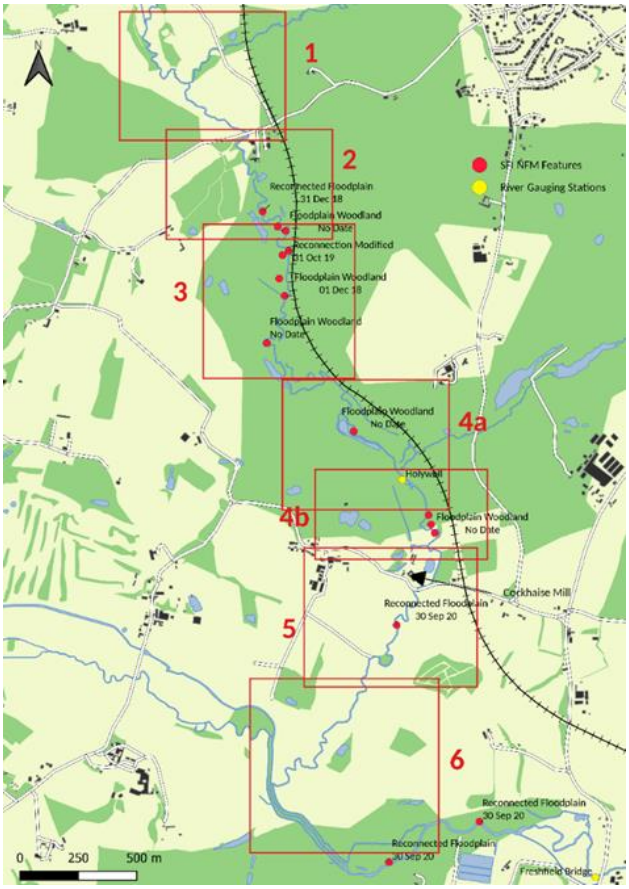

Figure 7:
The identified functional zones of Cockhaise Brook.

The evaluation was structured on the following spatial basis:

1. Detected flood area: comparison of flooding overall, by zone, and the immediate extent of the NFM features in Zones 2 to 5.
2. Flood form and location:
    a. Visual analysis of mapped flood coverage and form in each zone.
    b. Overall intersection analysis of both events to highlight locational changes in flooding.

c. Intersection of flood dispersal area in 20m incremental buffer rings from the brook, with pre- and post-NFM comparison to identify changes in distance from source.

3. Flood compactness: assessed by comparing the perimeter length of a convex hull drawn around the overall inundation extent.

As Sentinel-1 data frequency allowed only the pre-NFM event to be captured in ascendance *and* descendance, the evaluation assessed the two stages in aggregate and separately. It should be noted, however, that aggregating the extents may not depict the true extent of the flood at its peak.

To use these classifications in the evaluation, context is required. Increased flooding in certain areas is positive, for example where the NFM installation has created attenuation capacity. However, increases in flooding in a zone containing residential properties would be a negative outcome. Where no changes were detected, interpretation was required to assess the outcome. For example, where flood area was similar between the pre-NFM descendent stage and post-NFM, it was reasonable to assume that flooding had decreased.

3 Results

3.1 Ground Truth Flood Detection Rates

The Lee and Gamma MAP filters were tested on the ground truth sites, with results indicating no difference in flood detection rates between the filters in either dry or flood ground truth samples.

Table 4 sets out the percentage of ground truth polygons where open floodwaters and inundated vegetation were detected for the 20 December 2019 event. CDAT intersection analysis results for both calm (20 December) and windy conditions (21 December) on image differences against respective reference dates. The results of the intersection analysis are shown for known dry and flooded areas. Detection rates show few false positives in known dry areas (5.6 to 13.3%), but also low flood detection rates in areas of known inundation (53 to 56.5%).

Table 4: Flood detection rates in ground truth areas for the 20 December 2019 event.

Ground Truth Sample	Weather Conditions	Calm		Windy	
	Overall Area (ha)	20 Dec. 2019 vs 9 Nov. 2019 VH	20 Dec. 2019 vs 9 Nov. 2019 VV	21 Dec. 2019 vs 20 Nov. 2019 VH	21 Dec. 2019 vs 20 Nov. 2019 VV
		% Flood/Inundated Vegetation Detection			
Dry Ground Truth Total	122.57	5.6	9.8	9.5	13.3
Flood Ground Truth Total	101.84	53.0	53.4	56.5	55.6

Both polarizations demonstrate an increase in flood detection and false positives in windy conditions, although in VV the false positive increase outstrips the greater actual detection rates. Permanent water bodies were examined for their reaction in windy conditions. They exhibited an increase in image difference values, probably due to surface roughening, but this was not enough to qualify as a false positive.

Ground truth samples were taken across Sussex. Different geological and river characteristics were reflected in large variances in detection results for both polarizations and in both windy and calm conditions. Figure 8 shows a scatter graph of detection rates for sites representing dry conditions at the flood peak on 20 December. The floodwater detection rate is plotted horizontally. The vertical axis shows the variance from the peak flood on each particular river, which in this instance was the same date. The most significant observation is the relatively large proportion of false positives in VV polarization for Alfriston (28%) and Hellingly (20%).

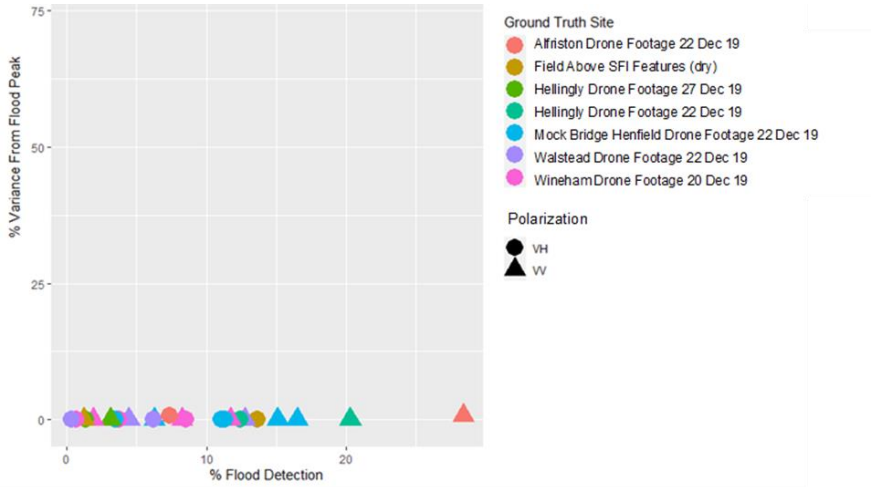

Figure 8: River level variance between the image date of 20 December 2019 and the local flood peak plotted against floodwater detection rates at ground truth sites representing dry areas during the event.

Representing known dry sites on 21 December 2019 against the baseline date of 20 November 2019, the scatter graph in Figure 9 shows how river levels vary from the local flood peak just one day later. High rates of flooding were also detected at these dry sample sites: 25% and 23% in VV and VH polarization respectively for Mock Bridge, and 20% in VV for Wineham.

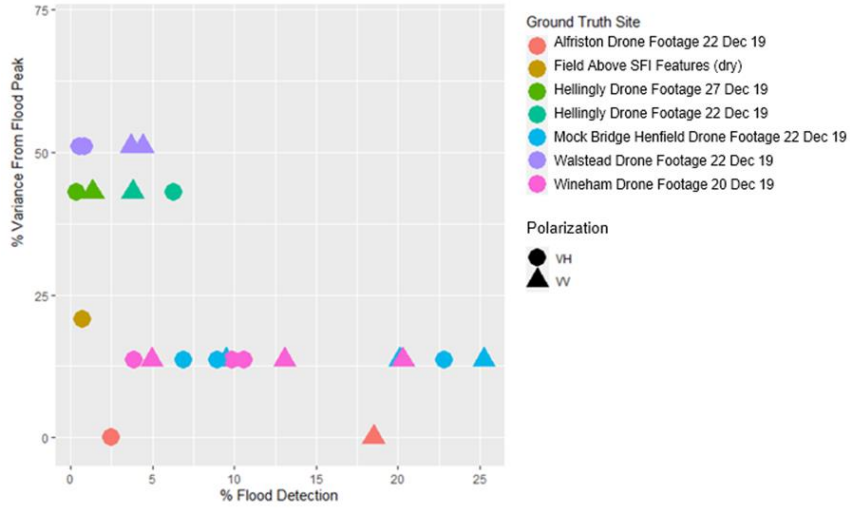

Figure 9: River level variance between the image date of 21 December and the local flood peak plotted against floodwater detection rates in ground truth sites representing dry areas during the event.

The scatter graphs of ground truth sites representing known flood coverage are shown in Figures 10 and 11 for the 20 December and 21 December respectively. For the 20 December image, except for Alfriston (both polarizations), there is a concentrated grouping of results between 42 and 96%. The spread of results for 21 December is far greater. Even without Hellingly (both polarizations) and the very small sample site of the NFM features, the range is from 10 to 82%.

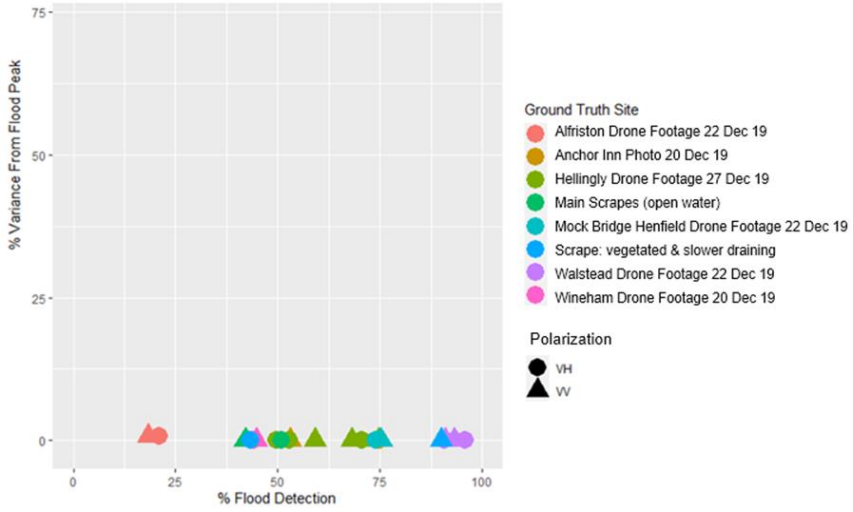

Figure 10: River level variance between the image date of 20 December 2019 and the local flood peak plotted against floodwater detection rates in ground truth sites representing flooding during the event.

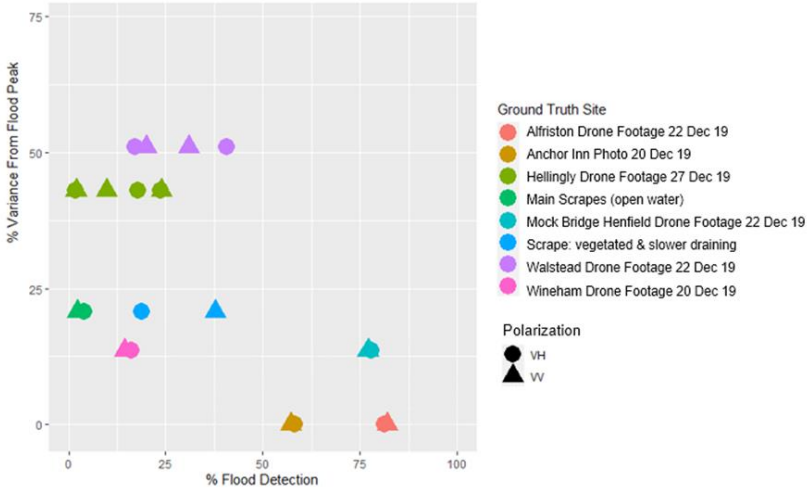

Figure 11: River level variance on the image date of 21 December 2019 to the local flood peak plotted against floodwater detection rates in ground truth sites representing flooding during the event.

3.2 Accuracy Assessment Results

Table 5 presents the optimum results of the intersection of floodwater and inundated vegetation in both dry and flood ground truth sites, in VH polarization, for the windy conditions of 21 December 2019 (29 km/h). Reducing the coefficient for inundated vegetation increased the number of false positives, without any beneficial increase in detected flooding. The optimum setting of 2.5 concurs with that used by Long et al. (2014). A reduction in the floodwater coefficient to 1.3 resulted in more false positives, but an increased flood detection rate generated an overall improvement in accuracy. Results in calm conditions were also more accurate in VH polarization, with a slightly different floodwater coefficient of 1.2.

Table 5: Confusion matrix for the ground truth sites using optimum CDAT coefficients in VH polarization in windy conditions, for the 21 December flood and reference of 20 November 2019.

Polarization:	**VH**			
Long Coefficient				
Flooded Vegetation:	**2.5**			
Floodwater:	**1.3**			
Flood Image Date:	**21/12/2019**			
Reference Image Date:	**20/11/2019**			
	Digitized References			
Sentinel-1 6am	**No Flood (ha)**	**Flood (ha)**	**Total (ha)**	**User's %**
No Flood ha	111.0	44.3	155.3	71.5%

Flood ha	11.6	57.6	69.2	83.2%
Reference Total ha	122.6	101.9	224.5	
Producer's %	90.5%	56.5%		
			Total Accuracy =	75.1%
			Kappa Statistic =	0.484

Overall, the total accuracy of the CDAT technique when optimum coefficients were employed was 75% in VH polarization. Further accuracy assessment matrix results in VV polarization and in calm conditions can be found in Jarrett (2022).

3.3 Cockhaise Brook Flood Detection Results

Detected Flood Area

Total areas of flood detection by functional zone are shown in Table 6, with the pre-NFM event peak represented in its ascendant and descendant stages.

Table 6: Detected areas of open floodwater/inundated vegetation by functional zone.

Functional Zone	Detected Flood Area (ha)		
	Pre-NFM Flood Event		Post-NFM Flood Event
	10 Jan. 2016 vs 5 Dec. 2015	13 Jan. 2016 vs 26 Nov. 2015	27 Nov. 2019 vs 9 Nov. 2019
1 North of Keysford Lane	0.52	0.55	2.13
2 Above main scrapes	0.16	0.40	0.35
3 Main scrapes	0.14	0.24	0.56
4a Below main scrapes to Danehill Brook	0.24	0.86	0.90
4b Danehill Brook to above Cockhaise Mill	0.01	0.34	0.05
5 Cockhaise Mill to Freshfield	0.13	1.49	1.87
Greater NFM Zone (zones 2–5)	0.68	3.33	3.73
6 Freshfield to Ouse	0.25	2.68	3.30
Total Cockhaise Brook	1.45	6.56	9.16

Based on aggregated totals for the pre-NFM event, substantial increases in flood area are evident in:

- Zone 1 – flood coverage has doubled from approx. 1ha to over 2ha post-NFM. However, this cannot be attributed to the flood management measures that were introduced as there is little change in Zone 2.
- Zone 3 – flood area has doubled from 0.24 ha to 0.56 hectares, reflecting the intention of the main scrapes, which was to attenuate inundation during peak flows.

Overall, across the zones containing NFM features (zones 2–5), flood area has not increased; in Zone 5 flooding immediately upstream of the residential area has largely been eliminated.

Flood Form

Figure 12 shows the overall flood extent for both pre- and post-NFM events by functional zone. Pre-NFM ascendant and descendant coverage are shown in aggregate. The key aspects of the maps comparing both events are the changes in area in Zones 1, 3 and 4. Flood form has changed in Zone 5, which includes the residential properties at Cockhaise Mill. A detailed analysis of locational changes in flooding on a zone-by-zone basis can be found in Jarrett (2022).

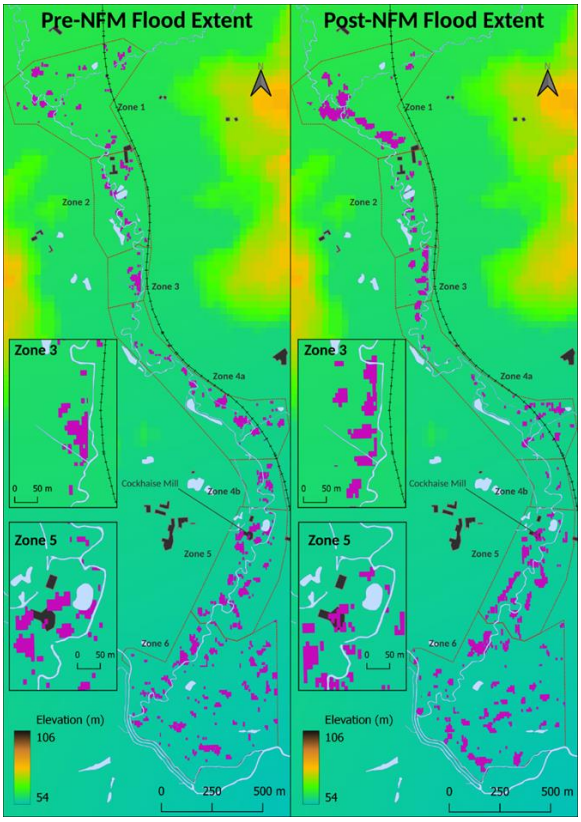

Figure 12:
Flood extent for the pre- and post-NFM events by functional zone.

Figure 13 shows the results of the GIS intersection analysis of pre- and post-NFM flood extent to identify specific locational changes. The results are segmented into different scenarios, as follows:

- Scenarios 1–3 identify areas of flood detected only in the pre-NFM event stages.
- Scenarios 4–6 identify areas of flood common to one or both of the pre-NFM stages *and* the post-NFM event.

Scenario 7 identifies areas of flood detected only in the post-NFM event.

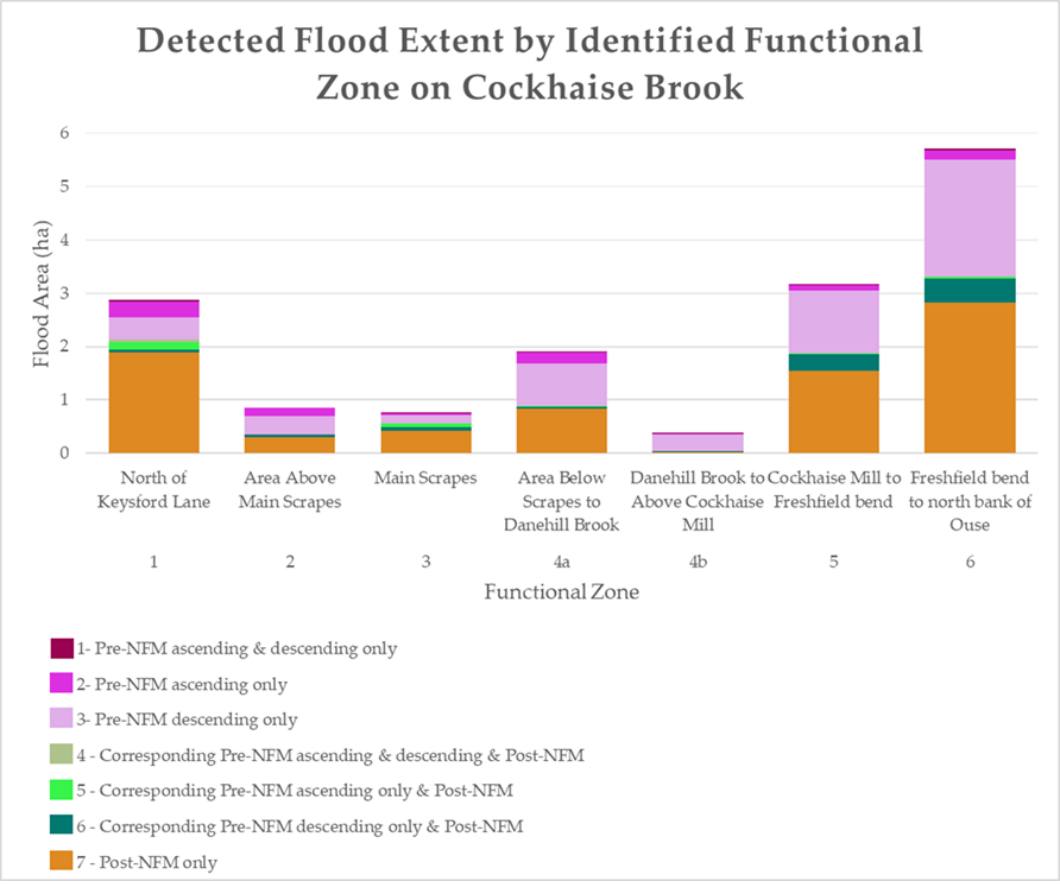

Figure 13: Common and singular extents of pre- and post-NFM flood events detected by functional zone.

A lack of coincidence between the two flood events can be seen in the predominance of pink and green in each zonal stack. This locational shift is supported by the increase in compactness that has occurred since the NFM installation (see Section "Flood Compactness").

Multi-buffer rings measure the total flood area around Cockhaise Brook covered by an event. It is clear from the scatter graph in Figure 14 that while the post-NFM flood area was greater (see Table 6), this area is concentrated within a distance of approximately 80m from the brook (i.e. is more compact in relation to Cockhaise Brook).

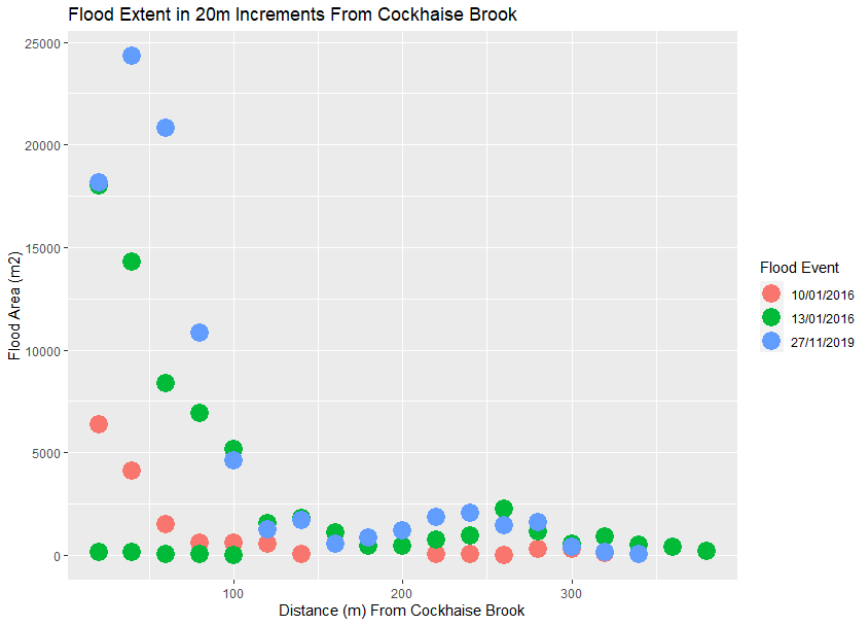

Figure 14: Inundated area at 20m increments away from Cockhaise Brook for the pre- and post-NFM flood events.

Flood Compactness

The overall compactness of flooding in each functional zone is summarized in Figure 15 using the perimeter length of a convex hull. There is very little difference in measurement of compactness between the flood events, despite the post-NFM event being larger in overall area.

3.4 NFM Evaluation Scorecard

Table 7 sets out the scorecard used to evaluate changes since the NFM installation on Cockhaise Brook against the three spatial flood characteristics. Five zones achieved positive results in flood extent, with 2 zones, north of Keysford Lane and around Cockhaise Mill, displaying negative changes; 4 zones exhibited positive changes in flood location and form, with negative change only in Zone 1. Finally, for compactness 4 zones recorded positive change, with no changes deemed to have had a negative effect.

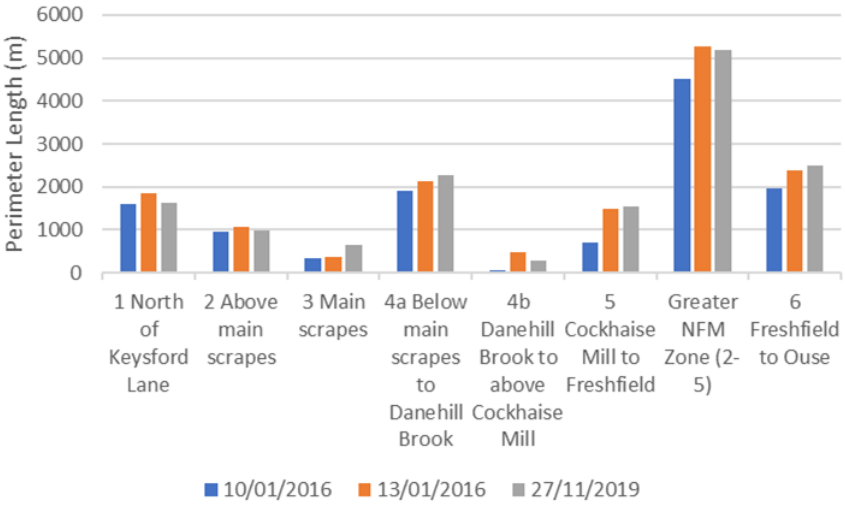

Figure 15: Perimeter length of overall flood extent for each functional zone based on a GIS-derived convex hull polygon.

Table 7: Final evaluation scorecard comparing pre- and post-NFM flood characteristics of detected area, form of flood extent and compactness by zone.

Functional Zone	Evaluation Criteria					
	Detected Flood Area		Form/Location of Flood Extent		Compactness	
	Status	Positive/ Neutral/ Negative	Status	Positive/ Neutral/ Negative	Status	Positive/ Neutral/ Negative
1 North of Keysford Lane	Increase	Neg	Change	Neg	Increase	P
2 Above main scrapes	Similar	Neu	Change	P	Similar	Neu
3 Main scrapes	Increase	P*	Change	P	Decrease	P*
4a Below main scrapes to Danehill Brook	Similar	P*	Change	Neu	Similar	Neu
4b Danehill Brook to above Cockhaise Mill	Decrease	P	Change	P	Increase	P
5 Cockhaise Mill to Freshfield	Increase	Neg	Change	Neu	Similar	Neu
Greater NFM Zone (zones 2–5)	Similar	P*	Change	P*	Similar	P*
6 Freshfield to Ouse	Similar	P*	Change	Neu	Similar	Neu
Positive Change Score		5/7		4/5		4/4

4 Discussion

4.1 Optimization of Histogram Threshold Settings

Optimum threshold settings to identify inundation extent applied equal weighting to maximizing detection in ground truth flood sites and minimizing detection in dry sites. The anticipated responses of open floodwater and inundated vegetation to the effects of wind on landscape surfaces were addressed by assessing accuracy in both windy and calm conditions. Wind *speed* was the overriding factor used to compare conditions, because it was not always possible to find comparable wind directions when speed was similar. It is acknowledged that gustiness could also have affected responses. VH polarization achieved the best results in both weather conditions considered.

Drone footage provided a suitable resource from which to establish ground truth polygons for both inundated and dry areas during a flood. However, analysis of the variance in detection rates highlighted some key issues affecting accuracy:

- Heterogeneous land cover was common for dry sites where there was a relatively large prevalence of false positives.
- Temporal lag between the SAR flood image date and the drone footage material is critical, as the larger this window, the more uncertainty is introduced.
- Pixels within ground truth sites representing known flood breaches where no inundation was detected displayed relatively high backscatter difference values, possibly indicating already-saturated ground in the reference image.
- Another factor that may affect detection in flood ground truth sites is the proximity of engineered river features, such as weirs.

If a project involving the assessment of spatial changes in flooding is to be evaluated, the overall project methodology should ideally include the identification of ground truth sites locally, as these provide examples of where flooding does and does not occur. While this might not be possible, the issues encountered in this research highlight some fundamental considerations in compiling a robust set of ground truth sites, namely: homogeneous land cover; any time lag between footage and the satellite image date should be as small as possible; similar site geology; awareness of engineered features affecting local flood characteristics; similar-sized sites to prevent undue skewing of results.

The main disadvantage of the detection methodology is that it produces low floodwater detection rates, therefore underestimating (rather than inaccurately representing) flood extent.

4.2 Evaluation of Post-NFM Flood Characteristic Changes

Although uncertainty is introduced by considering the pre-NFM total flood area in aggregate, it can be assumed that the actual peak flood coverage exceeded both the ascendant and

descendant totals. In the greater region of Zones 2–5 that contain the NFM features, despite floodwaters being deliberately attenuated post-NFM, the flood extent was similar.

At a zonal level, key changes were identified as follows:

- In Zone 1 there was a substantial increase in post-NFM flood extent, of 1.5 ha. Potential agricultural land-use changes around the northern section of the brook since 2016 may have increased run-off from adjacent land, inundating the brook in this location.
- Zone 4a displays the least degree of commonality between pre- and post-NFM flood inundation (3%) – a substantial shift in location. Zone 2 also has low coincidence of flood area. Significantly, zones 2 and 4a are both situated immediately adjacent to the main scrapes and display the smallest proportion of coincident flooding.
- Pre- and post-NFM flooding coincide most closely in Zone 3, where the main scrapes are situated. 18% of the total flood areas detected was coincident for both events. In this zone, flooding has increased post-NFM. As illustrated in Figure 12, the floodwater has generally been diverted into a managed space.
- Zone 5 contains the residential properties at Cockhaise Mill, for which the key aim of the project was to mitigate regular fluvial flooding. The residences are affected by pluvial surface water that compounds flooding north and south-west of the mill buildings. Figure 12 shows that, post-NFM, the inundation extent has decreased between the mill buildings and the brook.

In considering Zones 4b and 5 together, there is a possible combined effect of the main scrapes and nine other NFM features in these zones or immediately upstream changing certain flood characteristics on this section of Cockhaise Brook. Flood areas have decreased around Cockhaise Mill and immediately upstream by 0.5ha.

Overall, it is clear that the introduction of NFM installations has reduced flooding where intended and attenuated inundation in managed spaces, in line with design intentions, as demonstrated by the scorecard results. For all three indicators (flood area, flood form, and the compactness of the inundated extent), beneficial changes have outweighed any negative outcomes identified.

4.3 Sussex Flow Initiative: Use of Results

Research results were included in the SFI annual report for 2021/22 (SFI, 2022), citing how flood attenuation around the main scrapes in Zone 3 was in accordance with design intentions. The SFI Project Manager S. Buckland referred to 'the value of remote sensing to show changes in function' in feedback on the study (personal correspondence, 16 August 2022).

5 Conclusion

More scientific evaluation of any measures implemented needs to be undertaken to improve understanding of how NFM can be used in flood defence. Here, an evaluation methodology has been proposed that tests a scheme in extreme conditions. It is portable and simple in concept, suitable for supporting NFM design development, and relevant for small-scale floodplain restorations, as at Cockhaise Brook. Specific issues that were addressed in the SFI project, such as the surface water flows around Cockhaise Mill, are highly likely to occur in future evaluation work elsewhere. Such issues highlight the value of consultation to add technical insight in identifying positive and negative outcomes.

Key to the change detection methodology was to select comparable images of seasonally-similar significant flood events and benign river conditions. The long timescale between the pre- and post-NFM flood events selected was dictated by the short temporal windows of high river levels and the need to identify similar weather conditions. However, this introduced a greater likelihood of land-cover change, rather than NFM measures, affecting flooding.

The study results demonstrate how Cockhaise Brook has changed since the NFM installation during serious flood events. Flood extent has reduced immediately up- and downstream of the main scrapes, and flood water accumulation in the scrapes themselves has doubled, all without any increase in total flooded area.

References

Bernhardt, E. S., Palmer, M. A., Allan, J. D., Alexander, G., Barnas, K., Brooks, S., . . . Sudduth, E. (2005). Synthesizing U.S. River Restoration Efforts. Science, 308(5722), 636-637. doi:10.1126/science.1109769

Bioresita, F., Puissant, A., Stumpf, A., & Malet, J.-P. (2018). A Method for Automatic and Rapid Mapping of Water Surfaces from Sentinel-1 Imagery. Remote Sensing, 10(2). doi:10.3390/rs10020217

Brivio, P. A., Colombo, R., Maggi, M., & Tomasoni, R. (2002). Integration of remote sensing data and GIS for accurate mapping of flooded areas. International Journal of Remote Sensing, 23(3), 429-441. doi:10.1080/01431160010014729

Carreño Conde, F., & De Mata Muñoz, M. (2019). Flood Monitoring Based on the Study of Sentinel-1 SAR Images: The Ebro River Case Study. Water, 11(12), 2454. doi:10.3390/w11122454

Cian, F., Marconcini, M., & Ceccato, P. (2018). Normalized Difference Flood Index for rapid flood mapping: Taking advantage of EO big data. Remote Sensing of Environment, 209, 712-730. doi:10.1016/j.rse.2018.03.006

Clement, M. A., Kilsby, C. G., & Moore, P. (2018). Multi-temporal synthetic aperture radar flood mapping using change detection. Journal of Flood Risk Management, 11(2), 152-168. doi:10.1111/jfr3.12303

Environment Agency (2018). Working with Natural Processes – Evidence Directory. Bristol, UK

Environment Agency (2020). National Flood and Coastal Erosion Risk Management Strategy for England.

Green, K., Kempka, D., & Lackey, L. (1994). Using remote sensing to detect and monitor land-cover and land-use change. Photogrammetric Engineering and Remote Sensing, 60, 331-337.

HM Government (2018). A Green Future: Our 25 Year Plan to Improve the Environment. London

Huang, C., Chen, Y., Zhang, S., & Wu, J. (2018). Detecting, Extracting, and Monitoring Surface Water From Space Using Optical Sensors: A Review. Reviews of Geophysics, 56(2), 333-360. doi:10.1029/2018RG000598

Jarrett, S. E. (2022). Application of SAR Change Detection to Evaluate Flood Event Characteristics Pre and Post Restoration of a Floodplain. UNIGIS Master Thesis. Salzburg, Austria.

Kasischke, E. S., Melack, J. M., & Craig Dobson, M. (1997). The use of imaging radars for ecological applications—A review. Remote Sensing of Environment, 59(2), 141-156. doi:10.1016/S0034-4257(96)00148-4

Klemas, V. (2015). Remote Sensing of Floods and Flood-Prone Areas: An Overview. Journal of Coastal Research, 31, 1005-1013. doi:10.2112/JCOASTRES-D-14-00160.1

Long, S., Fatoyinbo, T. E., & Policelli, F. (2014). Flood extent mapping for Namibia using change detection and thresholding with SAR. Environmental Research Letters, 9(3), 035002. doi:10.1088/1748-9326/9/3/035002

Lu, D., Mausel, P., Brondízio, E., & Moran, E. (2004). Change detection techniques. International Journal of Remote Sensing, 25(12), 2365-2401. doi:10.1080/0143116031000139863

Macleod, R. D., & Congalton, R. G. (1998). A Quantitative Comparison of Change-Detection Algorithms for Monitoring Eelgrass from Remotely Sensed Data. Photogrammetric Engineering & Remote Sensing, 64(3), 207-216.

Manjusree, P., Prasanna Kumar, L., Bhatt, C. M., Rao, G. S., & Bhanumurthy, V. (2012). Optimization of threshold ranges for rapid flood inundation mapping by evaluating backscatter profiles of high incidence angle SAR images. International Journal of Disaster Risk Science, 3(2), 113-122. doi:10.1007/s13753-012-0011-5

Martinis, S., & Rieke, C. (2015). Backscatter Analysis Using Multi-Temporal and Multi-Frequency SAR Data in the Context of Flood Mapping at River Saale, Germany. Remote Sensing, 7(6), 7732-7752. doi:10.3390/rs70607732

Matgen, P., Hostache, R., Schumann, G., Pfister, L., Hoffmann, L., & Savenije, H. H. G. (2011). Towards an automated SAR-based flood monitoring system: Lessons learned from two case studies. Physics and Chemistry of the Earth, Parts A/B/C, 36(7), 241-252. doi:10.1016/j.pce.2010.12.009

SFI, S. F. I. (2022). Natural Flood Management Project End of Year Report 2021/22. Retrieved from http://www.sussexflowinitiative.org/uploads/1/6/3/1/16313516/sfi_eoy_report_21-22_final.pdf

Singh, A. (1989). Review Article Digital change detection techniques using remotely-sensed data. International Journal of Remote Sensing, 10(6), 989-1003. doi:10.1080/01431168908903939

van Rees, C. B., Naslund, L., Hernandez-Abrams, D. D., McKay, S. K., Woodson, C. B., Rosemond, A., . . . Wenger, S. J. (2022). A strategic monitoring approach for learning to improve natural infrastructure. Science of The Total Environment, 832, 155078. doi:10.1016/j.scitotenv.2022.155078

Zhang, B., Wdowinski, S., & Gann, D. (2022). Space-Based Detection of Significant Water-Depth Increase Induced by Hurricane Irma in the Everglades Wetlands Using Sentinel-1 SAR Backscatter Observations. Remote Sensing, 14(6), 1415. doi.org/10.3390/
rs14061415

Zhou, Y., Dong, J., Xiao, X., Xiao, T., Yang, Z., Zhao, G., . . . Qin, Y. (2017). Open Surface Water Mapping Algorithms: A Comparison of Water-Related Spectral Indices and Sensors. Water, 9, 256. doi:10.3390/w9040256